JOURNAL OF GEOPHYSICAL RESEARCH, VOL. 112, C10009, doi:10.1029/2007JC004227, 2007

Refraction and reflection of infragravity waves near submarine canyons

Jim Thomson,[1] Steve Elgar,[2] T. H. C. Herbers,[3] Britt Raubenheimer,[2] and R. T. Guza[4]

Received 19 March 2007; revised 28 June 2007; accepted 9 July 2007; published 10 October 2007.

[1] The propagation of infragravity waves (ocean surface waves with periods from 20 to 200 s) over complex inner shelf (water depths from about 3 to 50 m) bathymetry is investigated with field observations from the southern California coast. A wave-ray-path-based model is used to describe radiation from adjacent beaches, refraction over slopes (smooth changes in bathymetry), and partial reflection from submarine canyons (sharp changes in bathymetry). In both the field observations and the model simulations the importance of the canyons depends on the directional spectrum of the infragravity wave field radiating from the shoreline and on the distance from the canyons. Averaged over the wide range of conditions observed, a refraction-only model has reduced skill near the abrupt bathymetry, whereas a combined refraction and reflection model accurately describes the distribution of infragravity wave energy on the inner shelf, including the localized effects of steep-walled submarine canyons.

Citation: Thomson, J., S. Elgar, T. H. C. Herbers, B. Raubenheimer, and R. T. Guza (2007), Refraction and reflection of infragravity waves near submarine canyons, *J. Geophys. Res.*, *112*, C10009, doi:10.1029/2007JC004227.

1. Introduction

[2] Infragravity waves (surface gravity waves with periods of 20 to 200 s) were first observed as a "surf beat" modulation coincident with groups of narrow-band swell (periods of 10 to 20 s) [*Munk*, 1949; *Tucker*, 1950]. Subsequent investigations have shown that infragravity waves are important to sediment transport near the shoreline [*Holman and Bowen*, 1982; *Bauer and Greenwood*, 1990], currents in the surfzone [*Sasaki et al.*, 1976; *Kobayashi and Karjadi*, 1996], oscillations in harbors [*Okihiro et al.*, 1993], and fluctuations in seismic records observed on the continental shelf [*Dolenc et al.*, 2005; *Webb*, 2007].

[3] Although infragravity motions can be produced by a time-varying break point [*Symonds et al.*, 1982], storm fronts [*de Jong et al.*, 2003], and tsunamis [*Okihiro and Guza*, 1996], the primary forcing is via nonlinear quadratic interactions between swell waves (i.e., the difference interactions between the neighboring swell components that also produce wave groups) [*Hasselmann*, 1962]. As waves enter shallow water, the quadratic nonlinear interactions approach resonance, and near the shore significant energy can be transferred from swell to infragravity motions over a few hundred meters of propagation [e.g., *Gallagher*, 1971; *Elgar and Guza*, 1985; *Herbers et al.*, 1995b; *Ruessink*, 1998]. Thus infragravity waves usually are small in the deep ocean (owing to shoaling and trapping), and increase as the water depth decreases, reaching heights of $O(1)$ m at the shoreline where they can dominate the wave field [e.g., *Huntley et al.*, 1981; *Guza and Thornton*, 1985].

[4] When the swell waves break and dissipate in the surfzone, the infragravity waves are released and propagate toward the shoreline as free waves [*Longuet-Higgins and Stewart*, 1962; *Herbers et al.*, 1995b]. In the surfzone, infragravity waves transfer some of their energy back to motions with higher frequencies [*Thomson et al.*, 2006; *Henderson et al.*, 2006], before reflecting from the shoreline [*Suhayda*, 1974; *Guza and Thornton*, 1985; *Nelson and Gonsalves*, 1990; *Elgar et al.*, 1994; *Sheremet et al.*, 2002]. Reflected infragravity waves radiate seaward as freely propagating waves, some of which leak out to deep water and some of which return to the shore as refractively trapped edge waves [e.g., *Eckhart*, 1951; *Huntley et al.*, 1981; *Oltman-Shay and Guza*, 1987].

[5] Although previous observations suggest that nearshore submarine canyons may have a strong effect on the distribution of infragravity wave energy [*Inman et al.*, 1976; *Huntley et al.*, 1981], most wave propagation models account only for refraction over smooth changes in bathymetry [e.g., *Munk and Traylor*, 1947; *O'Reilly and Guza*, 1993]. Here a refraction-only model is shown to have relatively poor skill predicting the infragravity energy observed near two steep submarine canyons on the southern California inner shelf. In contrast, a ray-tracing model that incorporates both refraction over smooth bathymetry and partial reflections from sharp changes in bathymetry [*Kirby and Dalrymple*, 1983; *Thomson et al.*, 2005] has relatively high skill predicting the infragravity energy observed on the

[1] Applied Physics Laboratory, University of Washington, Seattle, Washington, USA.
[2] Woods Hole Oceanographic Institution, Woods Hole, Massachusetts, USA.
[3] Department of Oceanography, Naval Postgraduate School, Monterey, California, USA.
[4] Scripps Institution of Oceanography, La Jolla, California, USA.

0148-0227/07/2007JC004227$09.00

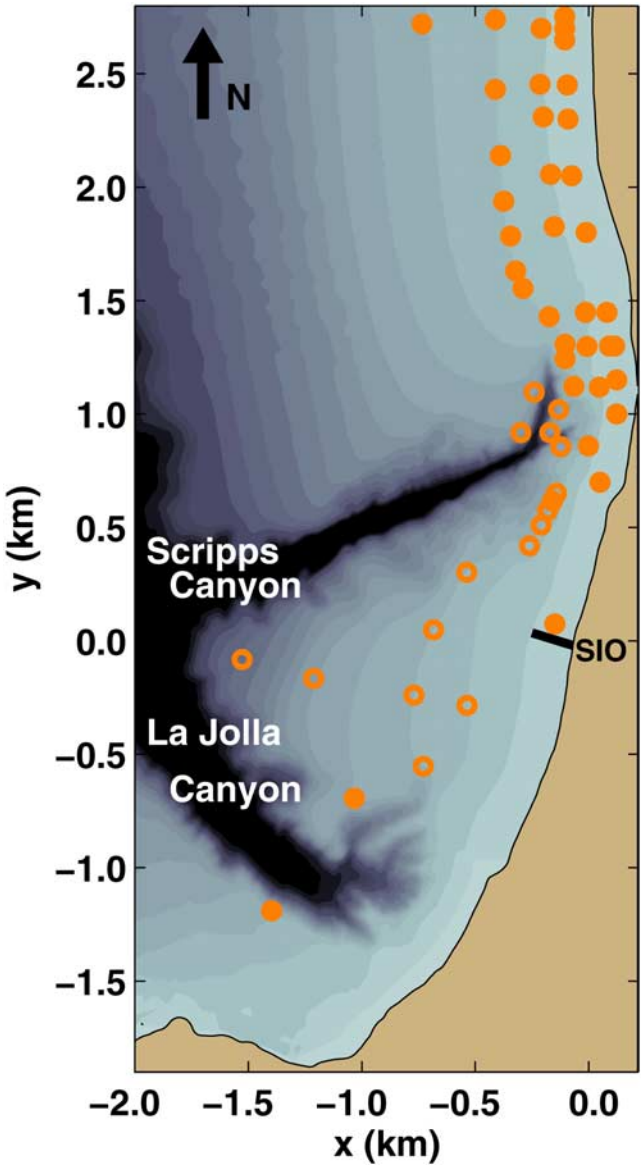

Figure 1. Instrument array (symbols) and bathymetry (shaded surface) using a local coordinate system (origin at the foot of the Scripps pier (SIO): 32.866°N, −117.256°W) along the southern California coast (tan region). Bottom-mounted instruments measured pressure (open symbols), and pressure colocated with velocity (solid symbols) during the fall of 2003. Water depths range from over 100 m (dark regions) in the Scripps (northern) and La Jolla (southern) canyons to 0 m at the shoreline (boundary between the lightest blue shading and the tan region). The alongshore arrays (symbols) are in approximately 2.5-, 5.0-, 10.0-, and 15.0-m water depths.

inner shelf and near the canyons for a wide range of conditions.

2. Field Observations

[6] An array of bottom-mounted current meters and pressure gages spanning a region near and onshore of two steep submarine canyons on the southern California shelf (Figure 1) was maintained from late September until late November, 2003. In depths h greater than 3 m, colocated pressure gages and acoustic Doppler current meters, as well as stand-alone (no colocated velocity measurements) pressure gages were mounted on fixed platforms within 1 m of the seafloor. In depths less than 3 m, the pressure gages were buried up to 1 m to prevent flow noise [*Raubenheimer et al.*, 1998]. Pressure and velocity data were collected hourly at 2 Hz for 3072 s (51 min) for 55 days, with brief interruptions for instrument maintenance, resulting in 1100 1-hour data runs with simultaneous records at each of the 52 instrument locations.

2.1. Data Processing

[7] After initial quality control to remove bad data [*Elgar et al.*, 2001, 2005], power and cross spectra of pressure and velocity with frequency resolution of df = 0.0068 Hz and 42 degrees of freedom (obtained by a combination of averaging the periodograms from 9 overlapping (by 75%) 1024-s-long Hanning-filtered windows and merging groups of 7 neighboring frequency bands [*Priestley*, 1981]) were estimated for each 1-hour data run. Spectra estimated with the near-bottom mounted pressure sensors were converted to sea-surface elevation using linear finite depth theory (accounting for exponential decay in the sand bed for buried sensors [*Raubenheimer et al.*, 1998]), and infragravity energy was estimated as the sum of surface-elevation variance (i.e., power spectra) over the frequency range $0.005 < f < 0.050$ Hz.

[8] Infragravity wave energy estimates in shallow water ($h < 3$ m) can be biased by contributions from shear instabilities of the alongshore current [*Oltman-Shay et al.*, 1989; *Bowen and Holman*, 1989], and thus the records (20% of the total) for which shear instabilities contributed more than 30% of the total infragravity velocity variance were excluded [*Lippmann et al.*, 1999]. The exclusion of cases with significant shear is important only for accurate model initialization (see section 3.2), because after initialization in shallow water, the wave propagation model was applied offshore ($h > 3$ m) of the typical shear region ($h < 3$ m).

2.2. Cross-Shore Energy Ratios

[9] Similar to previous results, observed total infragravity energy levels decrease offshore (Figure 2) as free waves with a dependence on depth h between the theoretical limits of $h^{-1/2}$ for a cross-shore propagating (leaky) wave field [*Elgar et al.*, 1992, Figure 3] and h^{-1} for an isotropic edge wave field [*Herbers et al.*, 1995a, Figure 7]. Contributions from forced, or group bound, waves that shoal proportional to a theoretical maximum h^{-5} ratio [*Longuet-Higgins and Stewart*, 1962] are small everywhere except the surfzone. Also similar to previous results, the relative contribution of seaward propagating leaky waves (with depth dependence $h^{-1/2}$) is estimated to be a significant portion of the total infragravity energy [*Sheremet et al.*, 2002].

[10] The observed energy ratios (Figure 2) are not described perfectly by either cross-shore leaky waves ($h^{-1/2}$) or isotropic trapped waves (h^{-1}), possibly because neither

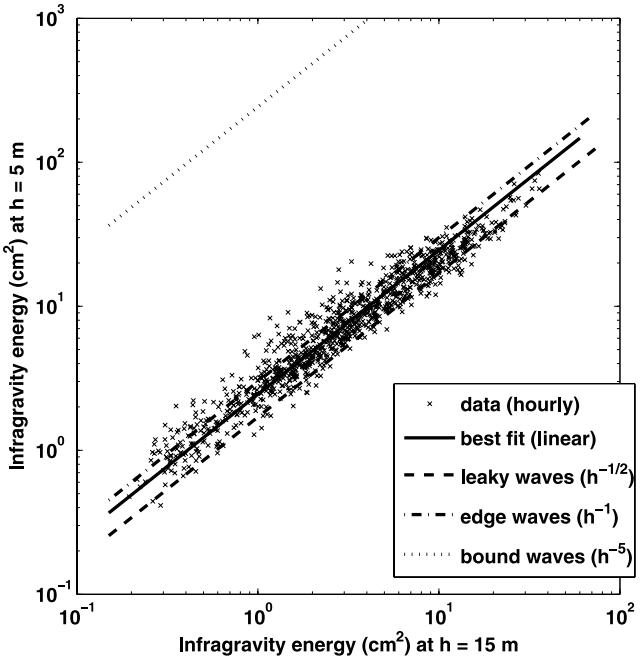

Figure 2. Infragravity energy (cm^2) observed in h = 5 m water depth versus infragravity energy (cm^2) observed in h = 15 m water depth along the northern cross-shore transect (y = 2.7 km, Figure 1). The least squares linear fit (solid line, ratio of 5- to 15-m-depth energy = 2.4, correlation = 0.95) to the hourly data (symbols) is between the theoretical $h^{-1/2}$ ratio of cross-shore propagating free waves (dashed line, ratio = $(5/15)^{-1/2}$ = 1.7) and the theoretical h^{-1} ratio of isotropic free edge waves (dash-dotted line, ratio = $(5/15)^{-1}$ = 3). The observations are far from the theoretical maximum h^{-5} ratio of cross-shore propagating forced waves (dotted line, ratio = $(5/15)^{-5}$ = 243). Some spread (less than 10%) about the values of 1.7 and 3.0 is expected owing to tidal fluctuations (1 m), which change ratios of instrument depths slightly (but not the absolute difference in depth).

estimate accounts for partial reflections by the canyons (Figure 1).

3. Wave Model

[11] Here a numerical model for the propagation over complex bathymetry of infragravity waves radiating from the surfzone is presented. The model propagates infragravity waves along individual ray paths, explicitly accounting for shoaling across the inner shelf, refractive trapping along the shoreline, and partial reflections from the Scripps and La Jolla submarine canyons. The approach is equivalent to tracing light rays from a distributed source through air and finite-width panes of glass.

[12] The model is initialized with observations from the seaward edge of the surfzone, and model predictions are compared with observations farther offshore. Thus infragravity energy on the shelf is assumed to be owing primarily to energy generated in less than 5-m water depth, reflected from the shoreline, and radiated seaward. Additional free wave energy from remote sources (e.g., surfzones across the Pacific Ocean [*Webb et al.*, 1991]), as well as local group-bound contributions, are assumed to be small.

3.1. Ray Tracing With Reflections

[13] The freely propagating waves are assumed to obey the linear, shallow-water dispersion relation

$$2\pi f = k\sqrt{gh}, \tag{1}$$

because at infragravity frequencies ($0.005 < f < 0.050$ Hz), the wavenumber magnitude k and the water depth h approach the nondispersive limit $kh \ll 1$ everywhere on the shelf ($h < 50$ m). Thus the wave energy and the wave phase propagate at a speed $c = \sqrt{gh}$, where g is gravitational acceleration.

[14] Rays are traced using

$$x_{n+1} = x_n + ds\cos(\theta_n), \quad y_{n+1} = y_n + ds\sin(\theta_n), \tag{2}$$

where x and y refer to cross-shore and alongshore directions, respectively (Figure 1), n is the integer number of ray segments along a ray path, ds is the length of a ray segment, and the angle θ is determined by refraction [*Mei*, 1989, section 3.2]

$$\theta_{n+1} = \theta_n + \frac{ds}{c}\left(\sin(\theta_n)\frac{\partial c}{\partial x} - \cos(\theta_n)\frac{\partial c}{\partial y}\right), \tag{3}$$

using the local depth $h = h(x_n, y_n)$. Using the shallow-water approximation (equation (1)), each ray transports a discrete wave packet with energy flux that is conserved along the path by shoaling and unshoaling proportional to $h^{-1/2}$. Errors introduced by neglecting finite depth effects on the dispersion relationship (equation (1)) are negligible for the results presented here, because rays leaving the outer edge of the surfzone (2.5 m depth) and subsequently intersecting the offshore sensors (located in less than 25 m depth) pass primarily through shallow water. While the energy of individual wave packets varies with $h^{-1/2}$, the total wave energy decreases more rapidly with increasing depth as more and more of the wave packets are trapped on the shelf, and in the limit of an isotropic wave field the total wave energy decays as h^{-1} [*Herbers et al.*, 1995a].

[15] Energy flux also is conserved at each canyon (Figure 3) where incident rays are split into partially reflected (at specular angles) and transmitted (angle conserved across the canyon) portions. Thus a canyon is a local partial reflector along a ray path, and the decrease in energy flux transmitted along the path is accounted for with a new reflected path. After splitting, each portion continues to refract until returning to the surfzone (secondary reflections are implicitly included in the initial conditions (section 3.2), and thus are not explicitly modeled) or reaching the deep water beyond the shelf (i.e., radiation condition at the offshore boundary).

[16] Observations of infragravity waves partially reflected at La Jolla submarine canyon [*Thomson et al.*, 2005] are well predicted by [*Kirby and Dalrymple*, 1983]

$$R^2 = \frac{\gamma}{1+\gamma}, \quad T^2 = \frac{1}{1+\gamma}, \tag{4}$$

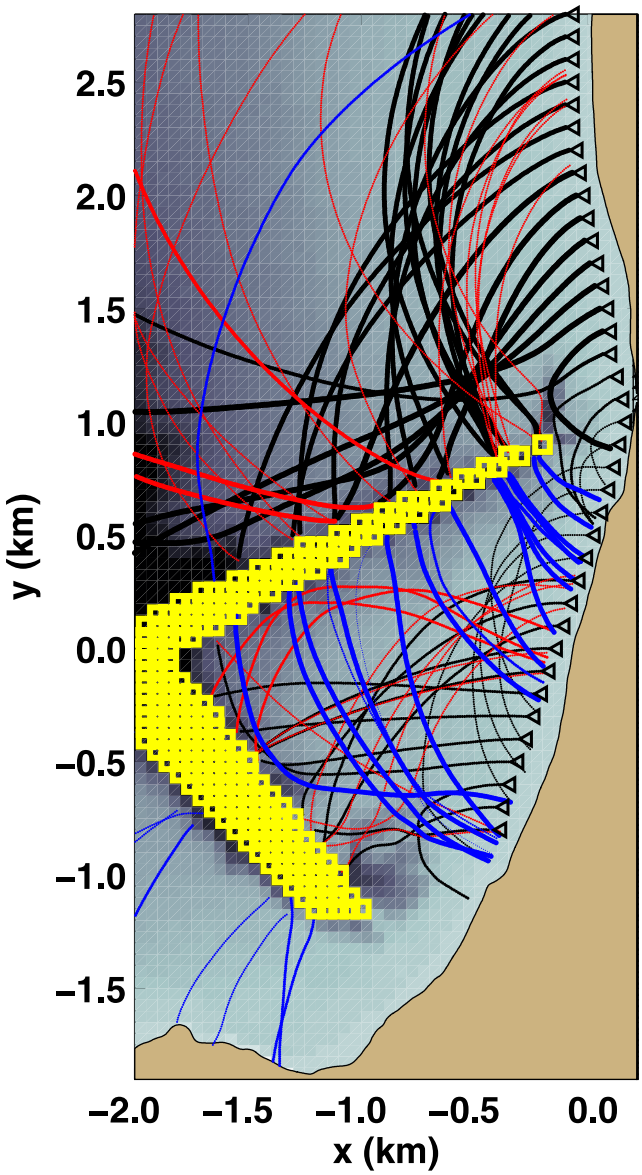

Figure 3. Ray paths (black curves) of 55-s period (f = 0.018 Hz) infragravity waves radiated seaward from the edge of the surfzone (black triangles ◁ along the 2.5-m isobath) at $\theta_0 = -25°$ from shore normal and refracted over gridded bathymetry. The model uses 50-m resolution, and every other (100-m separation) ray path is shown here. The width of each ray path is scaled by energy flux. Applying the long-wave theory (equations (4)–(5)), energy flux (and corresponding ray width) is conserved after initialization from observations in 2.5 m depth, and when rays are divided into partially reflected (red curves) and transmitted (blue curves) paths at the canyons (yellow grid cells). Ray paths are not defined over the canyons, which are approximated using rectangular cross sections that increase linearly in width (from 50 to 200 m for Scripps Canyon, and from 300 to 450 m for La Jolla Canyon) and depth (from 100 to 150 m for both canyons) with offshore distance.

and

$$\gamma = \left(\frac{h^2 l^2 - h_c^2 l_c^2}{2hlh_c l_c}\right)^2 \sin^2(l_c W), \tag{5}$$

where R^2 and T^2 are the ratios of reflected and transmitted energy, respectively, to the incident energy, and W is the canyon width using a rectangular approximation for each canyon cross section. The cross-canyon components of the wavenumber vector $\vec{k}$ in water depths within (h_c) and outside (h) each canyon are given by l_c and l, respectively. The wavenumber magnitude k is set by the shallow-water dispersion relation (equation (1)), and the components are determined using the value of θ_n at the edge of canyon such that $l = k \cos(\alpha - |\theta|)$, where α is the angle of the canyon axis relative to $\theta = 0$.

[17] For example, ray paths suggest that 55 s period (f = 0.018 Hz) infragravity waves propagating seaward from 2.5 m depth at an initial southerly angle $\theta_0 = -25°$ from the local shore-normal are partially reflected by Scripps canyon (Figure 3), reducing (increasing) the amount of wave energy that propagates southward (northward) along the shelf and refracts back to the shoreline. Evanescent modes, which decay with increasing distance from canyons, are implicit in calculating the net reflection and transmission (equations (4) and (5)), but are not assigned ray paths owing to their limited extent and effects [*Magne et al.*, 2007]. The energy flux of each ray is specified only at either side of the canyon, and thus the focus here is on the regional effects of the canyons and the interpretation of the field observations (all sensors were outside of the canyons, see Figure 1), rather than localized descriptions in the canyons (where waves are both propagating and evanescent, depending upon the angle of approach).

3.2. Initialization

[18] The model is initialized at each frequency using an energy flux directional distribution $\mathcal{F}(\theta_0, f)$ estimated from observations in 2.5 m depth (12 instruments along the shoreline in Figure 1). Assuming nearly shore-normal linear wave propagation close to shore, the total seaward energy flux $F(f)$ is estimated at each infragravity frequency f using the observations of pressure (P) and cross-shore (U) and alongshore (V) velocities as [*Sheremet et al.*, 2002]

$$F = \frac{\sqrt{gh}}{4}\left(PP + \frac{h}{g}(UU + VV) - 2\sqrt{\frac{h}{g}}PU\right), \tag{6}$$

where PP, UU, and VV are the autospectra of pressure and the velocity components, respectively, and PU is the cross-spectrum of pressure and cross-shore velocity.

[19] Normalized directional spectra $D_{\text{total}}(\theta_0)$ were obtained for each frequency using a Maximum Entropy Method (MEM) based on the first 4 Fourier coefficients of the directional spectrum estimated from the colocated observations of pressure and velocity [*Lygre and Krogstad*, 1986]. Although the MEM estimator resolves both seaward and shoreward propagating energy (Figure 4), only the seaward portion $D(\theta_0)$ is used for each ray initialization, consistent with the energy flux estimates. Phase-locked beach reflections are not accounted for by the MEM

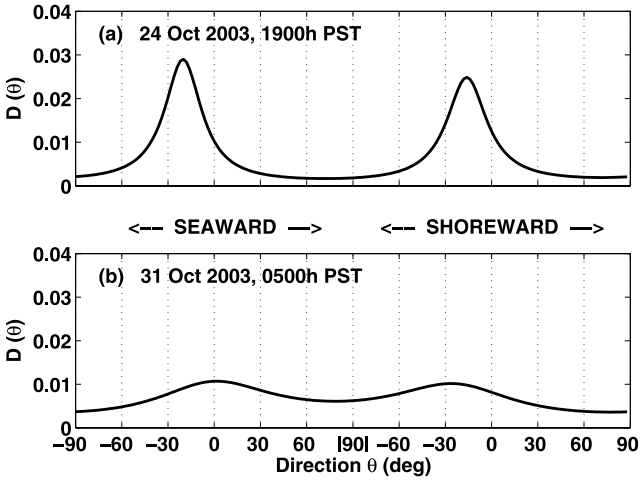

Figure 4. Normalized energy density at frequency f = 0.018 Hz (55-s period) versus direction (degrees relative to shore normal) for case studies with (a) narrow and (b) broad directional spectra $D(\theta_0)$ used to initialize seaward propagating ray paths. The directional spectra were estimated from observations in 2.5-m water depth at the north end of the array (x = −0.2 km, y = 2.7 km, Figure 1), and are qualitatively similar (i.e., narrow or broad) at all the infragravity frequencies ($0005 < f < 0.050$ Hz) and at all the 2.5-m-depth locations for each of the time periods shown. Only the seaward (left half of the figure) portion is used to initiate the model, and the directional spectra are rescaled to distribute the total seaward flux into $d\theta_0 = 5°$ bins for ray path initialization such that $\sum_{-90°}^{+90°} D(\theta_0) \cdot d\theta_0 = 1$. The centroid ($\theta_0$ = −25°) of the seaward-propagating peak in the directional spectrum in Figure 4a is used to initialize the example rays in Figure 3.

estimator, but significant standing wave modulations were not observed, possibly because the phase-locking effects are smoothed out by directional spreading, the relatively wide frequency bands, and surfzone nonlinearity and dissipation. Furthermore, tests using a different approach to estimate the directional spectrum (using a mean direction and the spread about the mean [*Kuik et al.*, 1988]) suggest that the results are insensitive to the directional estimation method. The directional distribution is normalized such that $\sum D(\theta_0) \cdot d\theta_0 = 1$, and thus $\mathcal{F}(\theta_0, f) = F(f)D(\theta_0)$.

[20] For each hourly data set, ray paths are initialized with evenly spaced (dl = 50 m) interpolations of discrete flux packets $\hat{\mathcal{F}} = \mathcal{F}(\theta_0, f) \cdot df \cdot d\theta_0 \cdot dl$ in each frequency-direction band ($d\theta_0 = 5°$ and df = 0.0086 Hz). To reduce effects from the edges of the finite domain, estimates of $\hat{\mathcal{F}}$ were extrapolated to initialize ray packets (also 50 m spacing) extending 1 km to the north and to the south of the 2.5-m-depth array (Figure 3). Ray packets were calculated for all nonzero components of $\mathcal{F}(\theta_0, f)$. The results are insensitive to the type (e.g., linear, quadratic, cubic spline) of interpolation used for producing initial conditions. The energy flux $\hat{\mathcal{F}}$ in each ray packet is conserved along the ray paths, regardless of changes in the bandwidth $d\theta$ (an advantage of the ray packet approach [*Bouws and Battjes*, 1982]) during refraction (equation (3)).

3.3. Regional Distribution

[21] To study the regional distribution of infragravity wave energy, ray paths are traced seaward from 2.5 m depth, and the corresponding flux packets $\hat{\mathcal{F}}$ are summed over a 50-m-resolution grid, assuming a linear superposition of the refracted wave components. The total infragravity energy E in a grid cell is calculated by summing flux contributions $E = \sum \hat{\mathcal{F}} \cdot T$ of discrete ray packets with residence times $T = \sum ds/c$ in that cell, where $c = \sqrt{gh}$ is the local group speed and ds is the length of a ray segment [*Bouws and Battjes*, 1982]. Several grid resolutions (25, 50, 100, 150 m) and ray segment lengths (ds = 5, 10, 20 m) were tested, with 50-m grid and 5-m ray segment values chosen as the best combination of accuracy and computational efficiency.

[22] Using the total infragravity energy simplifies the comparison with observations, and smoothes over any partial standing wave patterns that may be present near the canyons. Partial standing waves owing to the phase-coupling between incident and reflected waves are negligible in broadband wave fields near diffuse (i.e., sloping walls) reflectors [*Thomson et al.*, 2005], and are excluded in the phase-averaged tracing of rays.

4. Results

[23] The total infragravity energy predicted by the model is compared with the energy observed at the offshore instrument sites, which are grouped by depth for plotting. First, two contrasting case studies are described, and then a normalized root-mean-square error (i.e., model skill) is evaluated for the entire data set. The effects of partial reflection from the canyons are strongest within 1 km of the canyons.

4.1. Case Studies

[24] In a case study with a directionally narrow infragravity wave field radiated seaward (Figure 4a, 24 October 2003, 1900 h PST) from the surfzone at a mean angle θ_0 = −25° (south of shore normal), canyon effects are important to the distribution of infragravity energy on the inner shelf (Figure 5). For example, many of the θ_0 = −25° rays reach Scripps Canyon and reflect offshore to deep water (Figure 3), instead of propagating along the coast and contributing to the infragravity energy at southern sites (Figure 5). Similarly, many northward ($\theta > 0$, Figure 4a) rays reach Scripps Canyon and also reflect offshore (not shown). Thus the total infragravity energy at most sites is reduced by canyon reflections (Figure 5), even when southward components dominate (both southward and northward components are present for all cases).

[25] Although as large as a factor of four in places (e.g., y = 600 m on the 15-m isobath, Figure 5d), for this case study the difference in model skill (with and without reflections) is moderate, because Scripps canyon is narrow ($W \sim$ 100 m wide) relative to infragravity wavelengths ($2\pi/k \sim$ 500 m), and thus modeled reflections are small (<30%) for most angles of incidence (equations (4)–(5)). Canyon effects are more significant (e.g., reflections up to 95%) in the vicinity of the wider ($W \sim$ 350 m) La Jolla Canyon [*Thomson et al.*, 2005], but there are only a few locations with observations for comparison, and none for

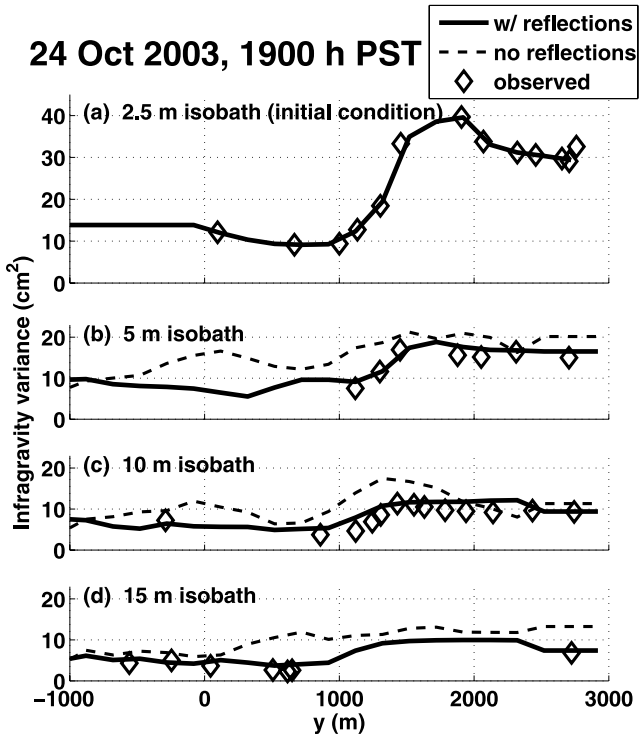

Figure 5. Observed (symbols) and modeled (curves) infragravity energy (cm^2) versus alongshore distance y (m) at four isobaths h = (a) 2.5, (b) 5.0, (c) 10.0, and (d) 15.0 m for 24 October 2003, 1900 h PST. In this directionally narrow case study (e.g., Figure 4a), a ray tracing model that includes partial reflection from the canyons (solid curves) has more skill than a refraction-only ray tracing model (dashed curves). The models are initialized by interpolating the estimated seaward propagating directional energy flux spectra $\mathcal{F}(\theta_0, f)$ along the 2.5-m isobath. The isobaths also vary in x (not shown) such that they wrap around each canyon (Figure 1), and thus modeled infragravity energy is defined at all points along the isobaths. For these depths, the Scripps and La Jolla Canyons are located between y = 650 to 900 m and $y = -1200$ to -800 m, respectively (Figure 3).

accurate surfzone initialization, south of the Scripps Pier ($y < 0.0$ km, Figure 1).

[26] In a case study with a directionally broad infragravity wave field radiated seaward (Figure 4b, 31 October 2003, 0500 h PST) from the surfzone at an angle $\theta_0 = 0°$ (shore normal), canyon effects are not as important to the distribution of infragravity energy on the inner shelf (Figure 6) as they are in the case with directionally narrow initial conditions (Figure 5). For the wave field with broad directional spectra, model predictions with and without reflections are similar to each other and to the observations (Figure 6). Other directionally broad case studies also exhibit a reduction in the impact of reflection on model skill compared with directionally narrow wave fields, possibly because the directionally broad distributions are mostly symmetric about shore normal (average $\theta_0 = -3°$). In contrast, the directionally narrow distributions have relatively more energy propagating southward (average $\theta_0 = -22°$), such that a larger percentage of the energy for the narrow cases intersects a canyon and is reflected.

[27] For all cases, the propagation of incident swell waves over complex bathymetry (not presented here) produces strong alongshore gradients of incoming energy in the surfzone [Kaihatu et al., 2002; A. Apotsos et al., Wave-driven setup and alongshore flows observed onshore of a submarine canyon, submitted to *Journal of Geophysical Research*, 2007], and the corresponding alongshore gradients of infragravity wave energy are important to the ray tracing initialization (e.g., Figures 5a and 6a). However, during the subsequent propagation (i.e., refraction and partial reflection) of infragravity waves, the alongshore gradients decrease with increasing water depth, producing nearly uniform alongshore distributions of energy in 10- to 15-m water depth (Figures 5c, 5d, 6c, and 6d). Thus, although the propagation of incident swell over the canyons has a large effect on the amount of energy available for local infragravity wave generation, it has a lesser effect on the overall distribution of infragravity energy in deeper water (i.e., on the inner shelf).

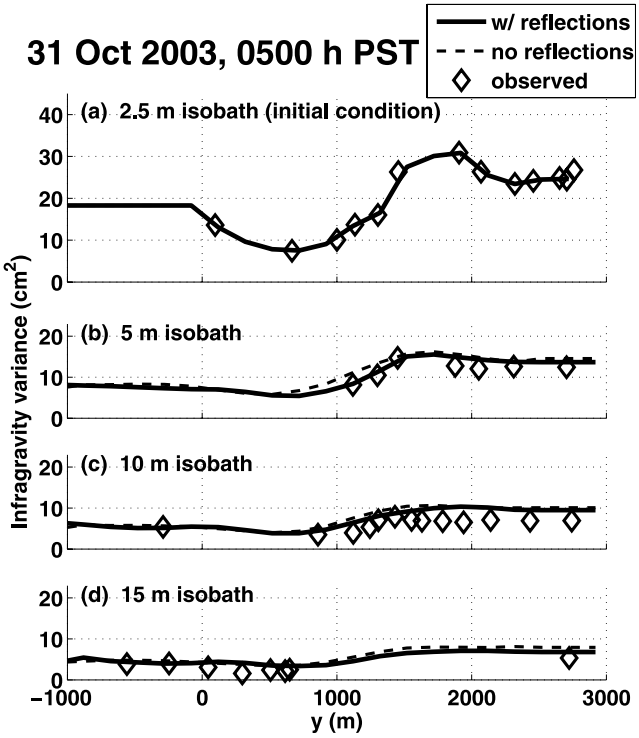

Figure 6. Observed (symbols) and modeled (curves) infragravity energy (cm^2) versus alongshore distance y (m) at four isobaths h = (a) 2.5, (b) 5.0, (c) 10.0, and (d) 15.0 m for 31 October 2003, 0500 h PST. In this directionally broad case study (e.g., Figure 4b), a ray tracing model that includes partial reflection from the canyons (solid curves) has equal skill to a refraction-only ray tracing model (dashed curves). The models are initialized by interpolating the estimated seaward propagating directional energy flux spectra $\mathcal{F}(\theta_0, f)$ along the 2.5-m isobath. The isobaths also vary in x (not shown) such that they wrap around each canyon (Figure 1), and thus modeled infragravity energy is defined at all points along the isobaths. For these depths, the Scripps and La Jolla Canyons are located between y = 650 to 900 m and $y = -1200$ to -800 m, respectively (Figure 3).

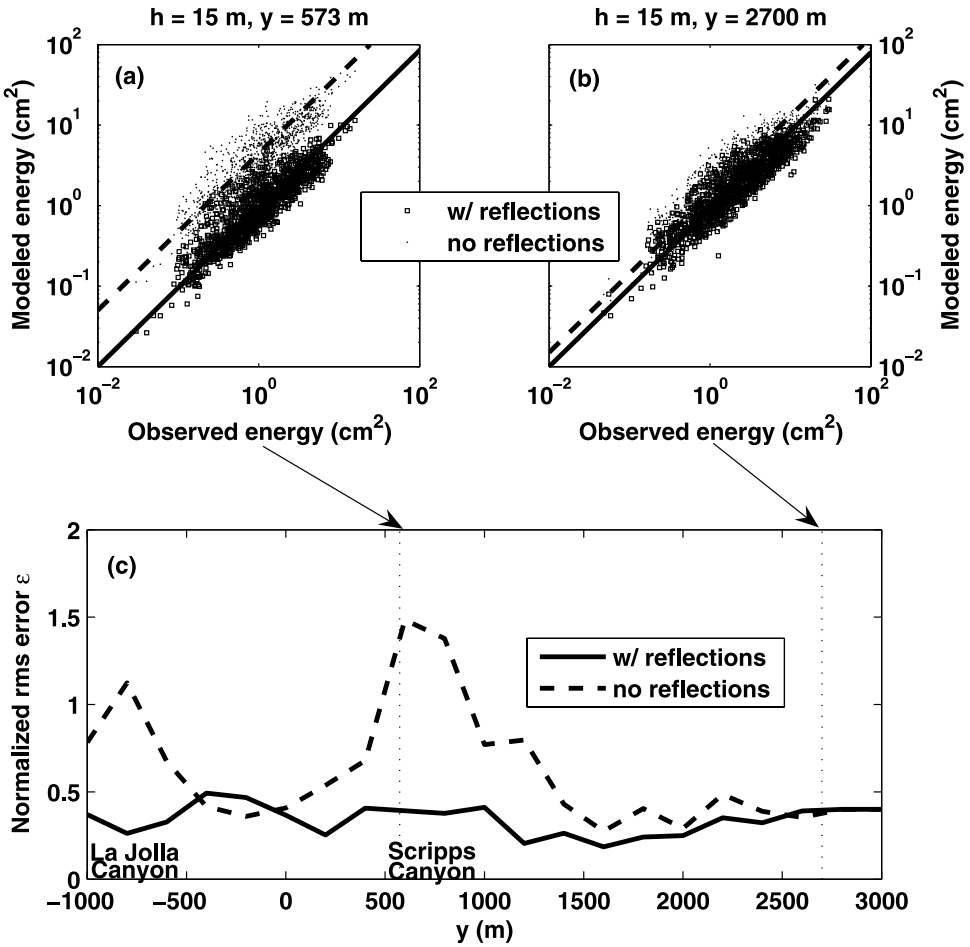

Figure 7. Modeled versus observed infragravity energy (cm^2) in 15-m water depth (a) near a canyon and (b) far from the canyons, and (c) normalized root-mean-square model errors versus alongshore distance. Results from the refraction model that includes canyon reflections (squares and solid best-fit lines) agree with observations at both locations (Figures 7a and 7b). Results from the refraction model that does not include canyon reflections (dots and dashed best-fit lines) agree better with observations at locations far from the canyons (Figure 7b) than at locations near a canyon, where the model overpredicts the observed energy by up to an order of magnitude (Figure 7a). The normalized root-mean-square error (averaged over all 40 sensors deeper than the 2.5-m-depth initial conditions and interpolated over the canyon axes) (Figure 7c) is small along the entire array for the refraction model with canyon reflections (solid curve), and is large in the vicinity of the La Jolla and Scripps canyons for the refraction-only model (dashed curve).

4.2. Model Skill

[28] Comparisons of model simulations with observations indicate that partial reflection from the canyons is important near Scripps Canyon where neglect of canyon effects can result in an order of magnitude overprediction of infragravity energy (Figure 7a) owing to the effectiveness of the canyon in deflecting infragravity waves offshore (and the subsequent wave radiation from the domain). However, far from the canyons, including canyon reflections results in significantly smaller improvement in model skill (Figure 7b). Averaging over all 1-hour records (880) and all offshore instrument locations (40 total, excluding initial conditions, but including several 20-m-depth instruments (Figure 1) not shown in Figures 5 and 6), accounting for partial reflections from the canyons results in improved model skill within about 1 km (i.e., a few wavelengths) of the canyons. In particular, a normalized model error ϵ, defined by

$$\epsilon = \sqrt{\frac{\sum(observed - modeled)^2}{\sum(observed)^2}}, \tag{7}$$

remains small near the canyons only if partial reflection is included in the ray-tracing model (Figure 7c). On average, the refracted-reflected ray tracing model explains 85% of the observed variance (defined as $100 \times [1 - \epsilon^2]$), whereas the refraction-only version explains 68% of the variance.

5. Conclusions

[29] The observed spatial variability of infragravity motions on a continental shelf with complex bathymetry

that includes two submarine canyons was analyzed with a wave propagation model that conserves energy flux during both refraction over smooth bathymetry and partial reflection from the canyons. The model was initialized with observations of seaward radiated infragravity waves generated within the surfzone along a southern California beach. The corresponding model predictions of infragravity energy on the inner shelf are in agreement with the field observations over a wide range of conditions. Comparisons of a refraction-only model and a combined refraction-reflection model with the observations suggest that the effects of submarine canyons on the spatial distribution of infragravity energy over the inner shelf primarily are localized to within a few wavelengths ($\sim$1 km for infragravity waves) of each canyon. Close to the canyons, the predictions of infragravity energy using a refraction-only model can be an order of magnitude greater than corresponding observed values. In contrast, the combined refraction-reflection model is accurate both near and far from the canyons.

[30] **Acknowledgments.** We thank field crews from the Woods Hole Oceanographic Institution, the Scripps Institution of Oceanography, Ohio State University, and the Naval Postgraduate School for their heroic efforts during data collection. Mark Orzech (Naval Postgraduate School) graciously provided the original refraction code, and Bill O'Reilly (Scripps Institution of Oceanography) helped gather observations and provided valuable comments about refraction over complex bathymetry. Funding was provided by the Office of Naval Research and the National Science Foundation.

References

Bauer, B. O., and B. Greenwood (1990), Modification of a linear bar-trough system by a standing edge wave, *Mar. Geol.*, *92*, 177–204.

Bouws, E., and J. A. Battjes (1982), A Monte Carlo approach to the computation of refraction of water waves, *J. Geophys. Res.*, *87*, 5718–5722.

Bowen, A., and R. A. Holman (1989), Shear instabilities of the mean longshore current: 1. Theory, *J. Geophys. Res.*, *94*, 18,023–18,030.

de Jong, M. P. C., L. H. Holthuijsen, and J. A. Battjes (2003), Generation of seiches by cold fronts over the southern North Sea, *J. Geophys. Res.*, *108*(C4), 3117, doi:10.1029/2002JC001422.

Dolenc, D., B. Romanowicz, D. Stakes, P. McGill, and D. Neuhausser (2005), Observations of infragravity waves at the Monterey ocean bottom broadband station (MOBB), *Geochem. Geophys. Geosyst.*, *6*, Q09002, doi:10.1029/2005GC000988.

Eckhart, C. (1951), Surface waves on water of variable depth, *Wave Rep. 100*, 99 pp., Scripps Inst. of Oceanogr., La Jolla, Calif.

Elgar, S., and R. T. Guza (1985), Observations of bispectra of shoaling surface gravity waves, *J. Fluid Mech.*, *161*, 425–448.

Elgar, S., T. H. C. Herbers, M. Okihiro, J. Oltman-Shay, and R. T. Guza (1992), Observations of infragravity waves, *J. Geophys. Res.*, *97*, 15,573–15,577.

Elgar, S., T. H. C. Herbers, and R. T. Guza (1994), Reflection of ocean surface gravity waves from a natural beach, *J. Phys. Oceanogr.*, *24*, 1503–1511.

Elgar, S., B. Raubenheimer, and R. T. Guza (2001), Current meter performance in the surfzone, *J. Atmosph. Oceanic Technol.*, *18*, 1735–1746.

Elgar, S., B. Raubenheimer, and R. T. Guza (2005), Quality control of acoustic Doppler velocimeter data in the surfzone, *Meas. Sci. Technol.*, *16*, 1889–1893.

Gallagher, B. (1971), Generation of surf beat by non-linear wave interactions, *J. Fluid Mech.*, *49*, 1–20.

Guza, R. T., and E. B. Thornton (1985), Observations of surf beat, *J. Phys. Oceanogr.*, *90*, 3161–3172.

Hasselmann, K. (1962), On the nonlinear energy transfer in a gravity-wave spectrum, 1, General theory, *J. Fluid Mech.*, *12*, 481–500.

Henderson, S. M., R. T. Guza, S. Elgar, T. H. C. Herbers, and A. J. Bowen (2006), Nonlinear generation and loss of infragravity wave energy, *J. Geophys. Res.*, *111*, C12007, doi:10.1029/2006JC003539.

Herbers, T. H. C., S. Elgar, and R. T. Guza (1995a), Infragravity-frequency (0.005–0.05 Hz) motions on the shelf, II, Free waves, *J. Phys. Oceanogr.*, *25*, 1063–1079.

Herbers, T. H. C., S. Elgar, and R. T. Guza (1995b), Generation and propagation of infragravity waves, *J. Phys. Oceanogr.*, *100*, 24,863–24,872.

Holman, R., and A. Bowen (1982), Bars, bumps, and holes: Models, *J. Geophys. Res.*, *87*, 12,749–12,765.

Huntley, D. A., R. T. Guza, and E. B. Thornton (1981), Field observations of surf beat: 1. Progressive edge waves, *J. Geophys. Res.*, *86*, 6451–6466.

Inman, D. L., C. E. Nordstrom, and R. E. Flick (1976), Currents in submarine canyons: An air-sea-land interaction, *Annu. Rev. Fluid Mech.*, *8*, 275–310.

Kaihatu, J. M., K. L. Edwards, and W. C. O'Reilly (2002), Model predictions of nearshore processes near complex bathymetry, paper presented at Oceans 2002, Inst. of Electr. and Electron. Eng., New York.

Kirby, J., and R. Dalrymple (1983), Propagation of obliquely incident water waves over a trench, *J. Fluid Mech.*, *133*, 47–63.

Kobayashi, N., and E. Karjadi (1996), Obliquely incident irregular waves in surf and swash zones, *J. Geophys. Res.*, *101*, 6527–6542.

Kuik, A., G. van Vledder, and L. Holthuijsen (1988), A method for routine analysis of pitch-and-roll buoy data, *J. Phys. Oceanogr.*, *18*, 1020–1034.

Lippmann, T. C., T. H. C. Herbers, and E. B. Thornton (1999), Gravity and shear wave contributions to nearshore infragravity motions, *J. Phys. Oceanogr.*, *29*, 231–239.

Longuet-Higgins, M. S., and R. W. Stewart (1962), Radiation stress and mass transport in surface gravity waves with application to surf beats, *J. Fluid Mech.*, *13*, 481–504.

Lygre, A., and H. E. Krogstad (1986), Maximum entropy estimation of the directional distribution in ocean wave spectra, *J. Phys. Oceanogr.*, *16*, 2052–2060.

Magne, R., K. A. Belibassakis, T. H. C. Herbers, F. Ardhuin, W. C. O'Reilly, and V. Rey (2007), Evolution of surface gravity waves over a submarine canyon, *J. Geophys. Res.*, *112*, C01002, doi:10.1029/2005JC003035.

Mei, C. C. (1989), *The Applied Dynamics of Ocean Surface Waves*, *Adv. Series on Ocean Eng.*, vol. 1, 740 pp., World Sci., Hackensack, N. J.

Munk, W. H. (1949), Surf beats, *Trans. AGU*, *30*, 849–854.

Munk, W. H., and M. A. Traylor (1947), Refraction of ocean waves: A process linking underwater topography to beach erosion, *J. Geol.*, *55*, 1–26.

Nelson, R. C., and J. Gonsalves (1990), A field study of reflections from an exposed dissipative beach, *Coastal Eng.*, *14*, 457–477.

Okihiro, M., and R. T. Guza (1996), Observations of seiche forcing and amplification in three small harbors, *J. Waterw. Port Coastal Ocean Eng.*, *122*, 232–238.

Okihiro, M., R. T. Guza, and R. J. Seymour (1993), Excitation of seiche observed in a small harbor, *J. Geophys Res.*, *98*, 2283–2319.

Oltman-Shay, J., and R. T. Guza (1987), Infragravity edge wave observations on two California beaches, *J. Phys. Oceanogr.*, *17*, 644–663.

Oltman-Shay, J., P. Howd, and W. Birkeimeir (1989), Shear instability of the mean longshore current: 2. Field observations, *J. Geophys. Res*, *94*, 18,031–18,042.

O'Reilly, W. C., and R. T. Guza (1993), A comparison of two spectral wave models in the Southern California Bight, *Coastal Eng.*, *19*, 263–282.

Priestley, M. B. (1981), *Spectral Analysis and Time Series*, 890 pp., Academic Press, San Diego, Calif.

Raubenheimer, B., S. Elgar, and R. T. Guza (1998), Estimating wave heights from pressure measured in sand bed, *J. Waterw. Port Coastal Ocean Eng.*, *124*, 151–154.

Ruessink, B. G. (1998), Bound and free infragravity waves in the nearshore zone under breaking and nonbreaking conditions, *J. Geophys. Res.*, *103*, 12,795–12,805.

Sasaki, T., K. Horikawa, and S. Hotta (1976), Observations of nearshore currents and edge waves, *Proc Coastal Eng. Conf.*, *16th*, Am. Soc. of Civ. Eng., Honolulu, Hawaii.

Sheremet, A., R. T. Guza, S. Elgar, and T. H. C. Herbers (2002), Observations of nearshore infragravity waves: seaward and shoreward propagating components, *J. Geophys. Res.*, *107*(C8), 3095, doi:10.1029/2001JC000970.

Suhayda, J. N. (1974), Standing waves on beaches, *J. Geophys. Res.*, *79*, 3065–3071.

Symonds, G., D. A. Huntley, and A. J. Bowen (1982), Two-dimensional surf beat long wave generation by a time-varying breakpoint, *J. Geophys. Res.*, *87*, 492–499.

Thomson, J., S. Elgar, and T. H. C. Herbers (2005), Reflection and tunneling of ocean waves observed at a submarine canyon, *Geophys. Res. Lett.*, *32*, L10602, doi:10.1029/2005GL022834.

Thomson, J., S. Elgar, B. Raubenheimer, T. H. C. Herbers, and R. T. Guza (2006), Tidal modulation of infragravity waves via nonlinear energy losses in the surfzone, *Geophys. Res. Lett.*, *33*, L05601, doi:10.1029/2005GL025514.

Tucker, M. (1950), Surf beats: Sea waves of 1 to 5 minute period, *Proc. R. Soc., Ser. A*, *202*, 565–573.

Webb, S. C. (2007), The Earth's 'hum' is driven by ocean waves over the continental shelves, *Nature*, *445*, 754–756, doi:10.1038/nature05536.

Webb, S., X. Zhang, and W. Crawford (1991), Infragravity waves in the deep ocean, *J. Geophys. Res.*, *96*, 2723–2736.

S. Elgar, Applied Ocean Physics and Engineering Department, MS 11, Woods Hole Oceanographic Institution, Woods Hole, MA 02543, USA. (elgar@whoi.edu)

R. T. Guza, Scripps Institution of Oceanography, UCSD Mail Code: 0209, 9500 Gilman Drive, La Jolla CA, 92093, USA. (rtg@coast.ucsd.edu)

T. H. C. Herbers, Department of Oceanography, Code OC/He, Naval Postgraduate School, Monterey, CA 93943, USA. (thherber@nps.edu)

B. Raubenheimer, Applied Ocean Physics and Engineering Department, MS 12, Woods Hole Oceanographic Institution, Woods Hole, MA 02543, USA. (britt@whoi.edu)

J. Thomson, Applied Physics Laboratory, University of Washington, 1013 NE 40th St., Seattle, WA 98117, USA. (jthomson@apl.washington.edu)